Near-THz Gyrotron: Theory, Design, and Applications

Contents

Introduction 3
Terahertz Gyrotron Program: 3
Detecting Concealed Sources: 4
THz Field (other attempts) 4
Gyrotron Operation 6
Gyrotron Parameters 8
Frequency/Power Requirement/Mode Choice 8
Terahertz Gyrotron 10
Cavity Design 10
General Theory 10
MAGY code simulation 11
Plasma Break Down 15
Gyrotron Theories 16
Guiding Center Spread 16
Frequency Tunability 19
Second Harmonic Interaction 21
Summary 21
Work Cited 22

Introduction

The proposed topic for my doctorate research is the study of theory of gyrotron devices related to sub-terahertz gyrotron program sponsored to detect radioactive sources through RF air breakdown. This proposal is composed of the following section:

I. Introduction
   a. Gyrotron program overview
   b. Background of gyrotron Physics
II. Sub THz Gyrotron
   a. Interaction circuit design
   b. Plasma breakdown
III. Gyrotron Theory
   a. Guiding Center Spread
   b. Excitation Tapered Waveguide
   c. Second Harmonic Gyrotron

This proposal will outline research that has been completed to date, and it will describe future efforts to be taken to complete the Ph. D thesis.

Terahertz Gyrotron Program:

When the Center for Applied Electromagnetics was established in 2008, one of the research tasks was to develop a THz gyrotron for the purpose of detecting concealed radioactive materials [1]. The gyrotron [2] is part of a scheme that is envisioned to create air breakdown using a focused wave beam in presence of free electrons. The underlying idea is that if a RF field with enough intensity can be focused in a region where there is a probability of accelerating a free electron, avalanche breakdown can result through electron collision. The presence of additional radioactive sources can amplify the background electron intensity by many orders of magnitude over the ambient background free electron density, which is about one particle per cubic centimeter; ambient free electrons are usually created through cosmic rays and radioactive elements in the environment.

Detecting Concealed Sources:

For example, a common radioactive source, Colbalt-60, is shown to have gamma emission of 1.173 MeV and 1.3325 MeV [2]. The two spectrum emission peaks occur simultaneously with equal probability. Given moderate shielding such as a steel shipping container, a gamma ray will propagate through the wall and ionize air, which will in turn create secondary electrons and so on.
The difference between background free electron density and the additional electron density due to radioactive sources will be the key in detecting the presence of the radioactive sources. The proposed method of using THz wave allows us to focus the RF field in a small volume less than $1cm^3$, such that the probability for presence free electron is very low without the additional presence of radioactive sources; thus, breakdown is unlikely. If a radioactive source is present, then the chance of breakdown will be much higher, and diagnostics can be designed to measure the breakdown probability leading to a detection scheme for radioactive sources.

This sets apart the proposed breakdown study from previous breakdowns with microwave and optical sources. Previous works with microwave breakdown had been done at much lower frequencies, where the focusing volume is so large that there would almost always be free electrons present in the focusing region [3] [4] [5]. At the optical regime, the lasers have enough energy per photon that multi-photon ionization will occur for neutral atoms even in absence of any free electron. The THz region is a relatively new area to explore this breakdown phenomenon.

THz Field (other attempts)

High power sources for the terahertz region had not been as actively developed compared to optical or microwave region. Figure 1 shows that while vacuum devices have existed for high power uses and solid state devices have worked for high frequency, there is a gap of development for the terahertz region with high power. At present, there have been a slew of new activities aimed at this frequency range: recently, sub-millimeter wave device up to 1.4 THz [6] was demonstrated to be able to deliver milliwatt power in continuous operation. An earlier attempt with pulsed solenoid gyrotron was able to reach 500 GHz with 100kW, and it set a record of 8.2% efficiency [7]. More recently, a Russian team demonstrated pulsed gyrotron operation at 1-1.3 THz up to 5kW [8].

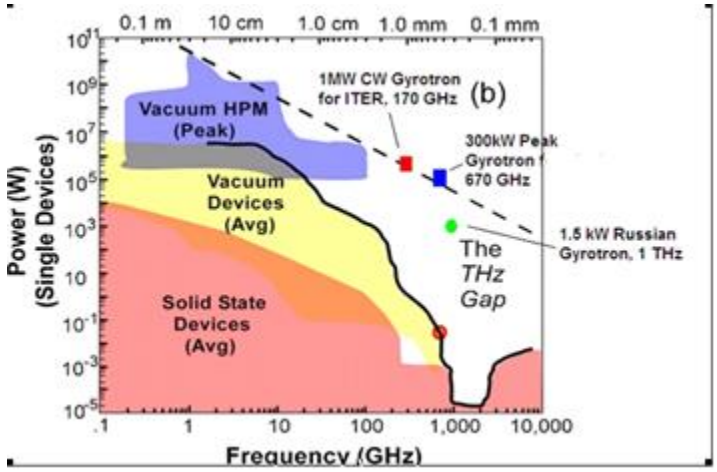

Figure 1 Radiation sources development

Second harmonic gyrotron development at 460 GHz frequency was reported in [9], the recent design of a 400 GHz third-harmonic gyrotron is described in [10]. The motivation for going to higher harmonic resonance is that gyrotron's frequency is directly proportional to magnetic field, as shown in figure 2, and even super conducting magnets with fields corresponding to an electron cyclotron frequency greater than 400 GHz are unavailable. Also, at high harmonic cyclotron resonance, the overall efficiency tends to be lower as compared to fundamental cyclotron resonance. FELs, while able to produce output high power in a very wide frequency range [11], are physically bulky and unsuited for field uses, where mobility may be a requirement.

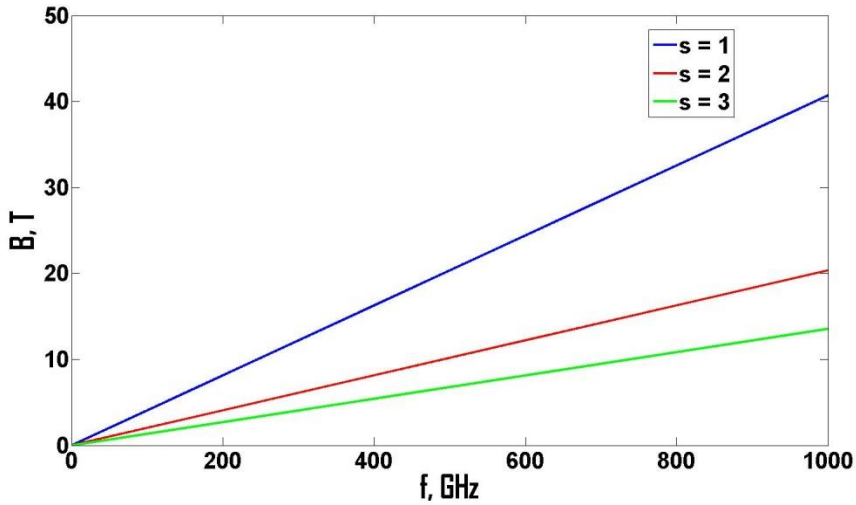

Figure 2 Gyrotron frequency vs. magnetic field, for different cyclotron harmonic number s

In order to obtain high efficiency and high power output at frequency greater than 400 GHz, we choose to pursue a gyrotron at the fundamental cyclotron resonance; one approach to achieve the required high magnetic field is to use a pulsed magnet.

Gyrotron Operation

In microwave devices, we distinguish between fast wave and slow wave devices [12]. Gyrotron is a class of relativistic fast wave devices that utilize electron cyclotron resonance and wave beam interaction to convert electron kinetic energy into radiation. As shown in figure 3, a typical gyrotron oscillator, or gyromonotron, typically consists of these major components:

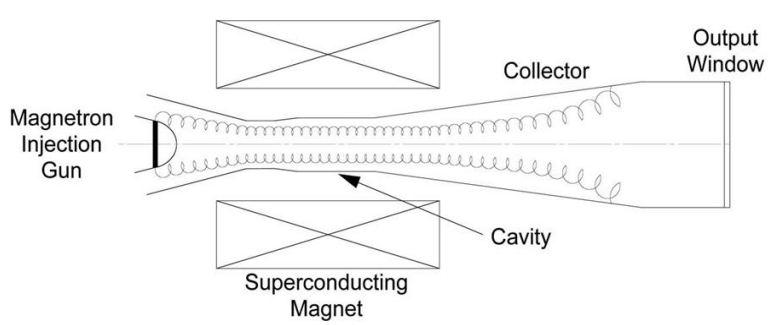

Figure 3 Simple Gyrotron Schematic

1) Electron source, such as a magnetron injection gun

2) Interaction circuits (Cavity)

3) Magnetic field source, (Magnets or Solenoids)

4) Spent electron beam collector

5) Output taper and window

Initially, the electron beam is injected from the gun into the cavity. The electrons are distributed along the gyro orbit randomly, with an initial perpendicular and axial velocity before any interaction takes place, see figure 4 (a). When the electrons encounter the magnetic field, electrons begin to rotate following the Lorentz force law. When this takes place in presence of a RF field, electrons experience acceleration or deceleration depending on their rotation phase. Since the electrons are accelerated to relativistic speed in the gun, the effective mass of the electron varies; in the cavity, some electrons accelerate and some decelerate, causing them to have slightly different cyclotron frequencies, which is given by $\Omega = \frac{eB_o}{m\gamma}$, as seen in figure 4 (b). Increase in Lorentz factor γ will reduce cyclotron frequency Ω, and vice versa. This effect can lead to electron bunching in the deceleration phase when wave frequency ω is greater than Ω, and energy can be transferred from the beam to the wave, shown in figure 4 (c).

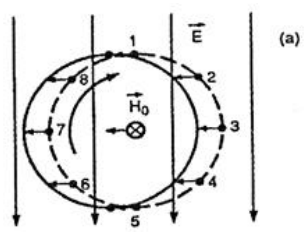

Figure 4 (a) Initial modulation

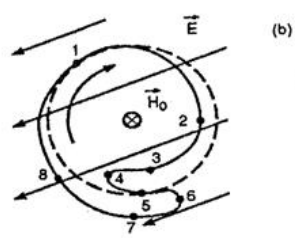

Figure 4 (b) Electron bunching

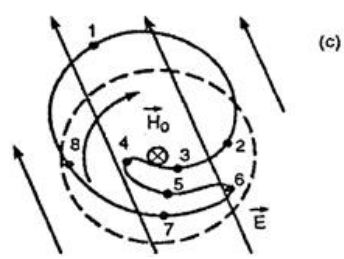

Figure 4 (c) Bunch deceleration

In general the cyclotron resonance condition is $\omega = k_z v_z + s\Omega$, where k_z is the axial wave number, v_z is the beam axial velocity, s is the harmonic number, which equals to 1 for the fundamental harmonic. The Doppler term $k_z v_z$ can be minimized by exciting the gyrotron cavity near cut-off of the dispersion curve where $k_z \approx 0$, see figure 5.

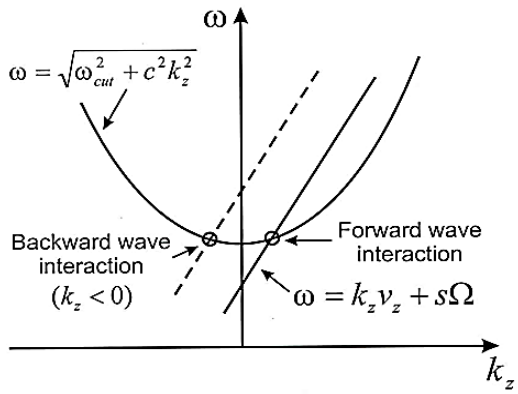

Figure 5 Gyrotron dispersion

Gyrotron Parameters

Frequency/Power Requirement/Mode Choice

Our proposed gyrotron is designed to operate at 670 GHz (the wavelength about 0.45 mm), and the gyrotron is designed to deliver power in the range of 100-200 kW in single-shot pulses. The microwave pulse duration designed to be about 10 microseconds. The choice of frequency is determined by 2 considerations. First, at this frequency, there is a relative transmission window in air where loss is at the 50 dB/km level as shown in figure 6. For a wave beam that propagates over a distance of about 20 m the wave power would be attenuated by about 1 dB [2].

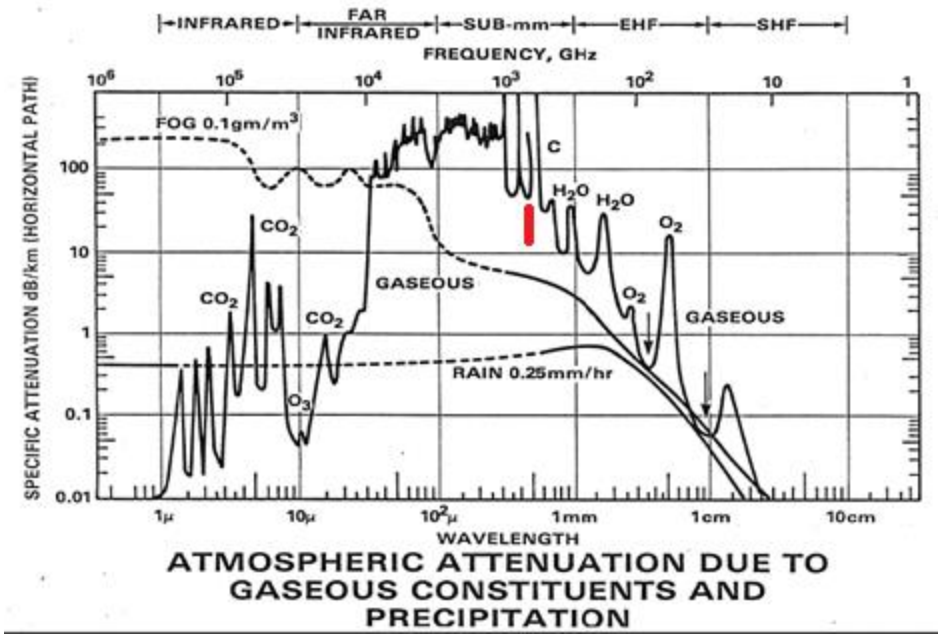

Figure 6 Atmospheric attenuation at high frequencies, red marks the 670GHz or 0.45 mm wavelength

The second reason is that in a related study, a relationship is described between the field intensity threshold for air breakdown and the frequency of the RF field [13]. Those calculations roughly translate to ~100 kW power needed near the bottom of the breakdown curve, roughly in the range of 670 GHz.

To compensate for the high wall losses in the cavity at such a high frequency, we look for a high order cavity mode. Recent gyrotron experiment for ITER [14] showed that $TE_{31,8}$ can be selectively excited and it operated stably. So we choose this mode in our design study.

Terahertz Gyrotron

Cavity Design

General Theory

In a simple version of the general gyrotron theory [12], the interaction efficiency can be defined as:

$$\eta_{\text{int}} = \left[\beta_{\perp 0}^2 / 2\left(1-\gamma_0^{-1}\right)\right]\eta_\perp$$

For cut-off operation, $\beta_{\perp 0} = v_{\perp 0} / c$ is the initial orbital velocity normalized to the speed of light, $\gamma_0 = 1 + eV_b / mc^2$ is the Lorentz factor determined by the beam voltage V_b and $\eta_\perp$ is the orbital efficiency characterizing the fraction of the energy of electron gyration transformed into electromagnetic radiation. When the axial structure of the resonator field is assumed not to be disturbed by an electron beam, orbital efficiency depends on four normalized parameters: normalized length $\mu = \pi\left(\beta_{\perp 0}^2 / \beta_{z0}\right)\left(L/\lambda\right)$, field profile $f(z)$, normalized cyclotron resonance mismatch Δ and the normalized beam current parameter I_0. For the beam voltage, orbital-to-axial velocity ratio and the cavity length chosen, the gyrotron's (70 kV, $\beta_{\perp 0} / \beta_{z0} = 1.2$, $L/\lambda = 10$) normalized length μ is equal to 14.4, which is close to the optimal value for gyrotrons with Gaussian axial structure of the cavity field. According to general theory, for any given mode with maximum beam wave coupling for the chosen parameter above, and optimal detuning, the maximum orbital efficiency, $\eta_\perp$, can be about 70% when the velocity spread is neglected. The efficiency, η_{int}, that corresponds to our choice of Q-factors, orbital velocity and the Lorentz factor specified above is approximately 35%.

As mentioned before, we choose to operate in a high order cavity mode in order to minimize the ohmic losses at high frequency. The power radiated by electrons is divided between the power of outgoing radiation, P_{out}, and the power of ohmic losses P_Ω. These are inversely proportional to the diffractive and ohmic quality factors, as given by

$$P_{out} = \left(\omega / Q_D\right)W \text{ and } P_\Omega = \left(\omega / Q_\Omega\right)W .$$

W is the energy stored in the cavity, the diffractive Q-factor $Q_D \approx 30\left(L/\lambda\right)^2$ is usually in the range between one to several thousand depending on the ratio of the resonator length L to the wavelength. $Q_\Omega = \left(R_w / \delta\right)\left(1 - m^2 / \nu_{m,p}^2\right)$, is the ohmic Q-factor of the $TE_{m,p}$-modes, R_w is the cavity wall radius, m

is the azimuthal index of the mode, p is the radial index, and $\upsilon_{m,p}$ is its eigen number. $\delta = \frac{1}{\sqrt{\pi f \sigma \mu_o}}$ is skin depth and σ is the conductivity of the cavity wall.

At the frequency of 670 GHz, for the $TE_{31,8}$ mode, the wall radius is 4.543 mm and the ohmic Q is approximately equal to 30,000. For normalized cavity length of 10, the diffractive Q is close to 3,000 and the resulting ohmic loss of power in the cavity wall should be about 10% or the radiated power.

MAGY code simulation

The self-consistent code MAGY [15] is used to test the basic cavity profiles shown in figure 7, and to perform simulation to find the optimal design: Figures 7 a-c have similar interaction length, the main difference is the up-taper between the cavity input and the interaction region. Figure 7a has a very abrupt transition; figure 7b has a linear up-taper; figure 7c has a smooth curve transition, where the up-taper angle is 5 deg.

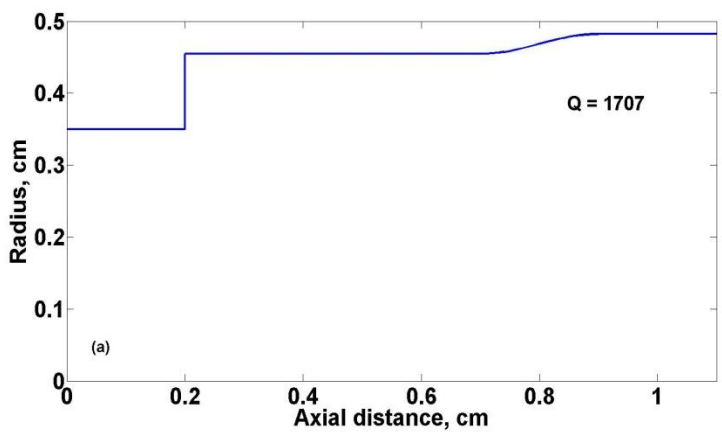

Figure 7 (a) Cavity Profile 1

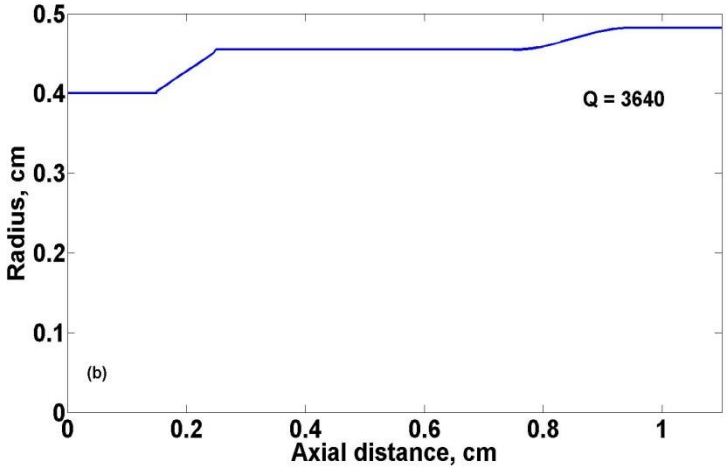

Figure 7 (b) Cavity Profile 2

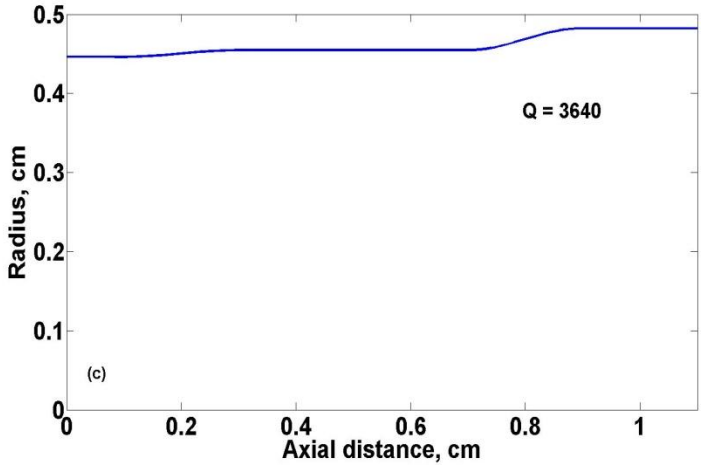

Figure 7 (c) Cavity Profile 3

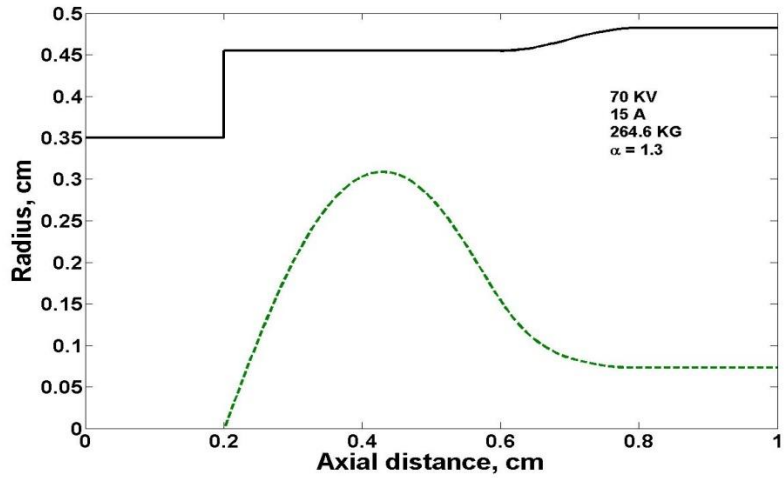

Figure 8 Axial Field Structure

MAGY simulations are shown in figure 8-9, for set of beam parameters. The axial field structure for cavity shown in figure 7 (a) is shown in figure 8. The efficiency as the function of the external magnetic field is shown in figure 9 for several values of the orbital velocity spread. Calculations were done for a 70 kV, 15A electron beam with the mean value of the orbital-to-axial velocity ratio 1.3. The results were obtained for the gyrotron with finite conductivity of the cavity wall. These results indicate that the gyrotron operations are relatively insensitive to the velocity spread: even the 10% RMS spread in orbital velocities would cause only small decline in the maximum efficiency. Further optimization of the resonator shape showed that the output efficiency can even be close to 35%, as shown in figure 9(c).

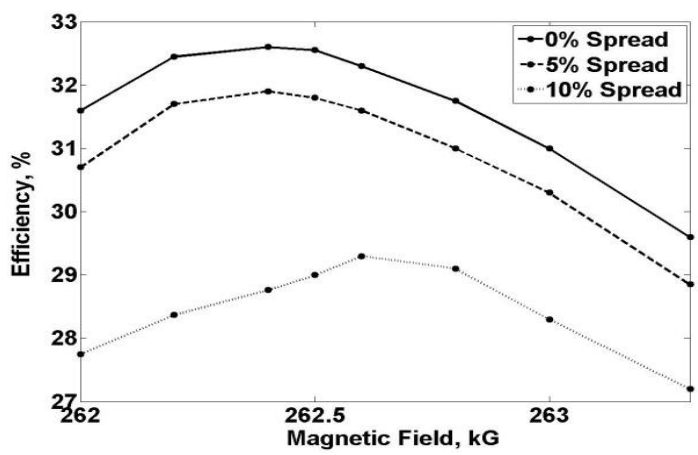

Figure 9 (a) Efficiency for profile 1

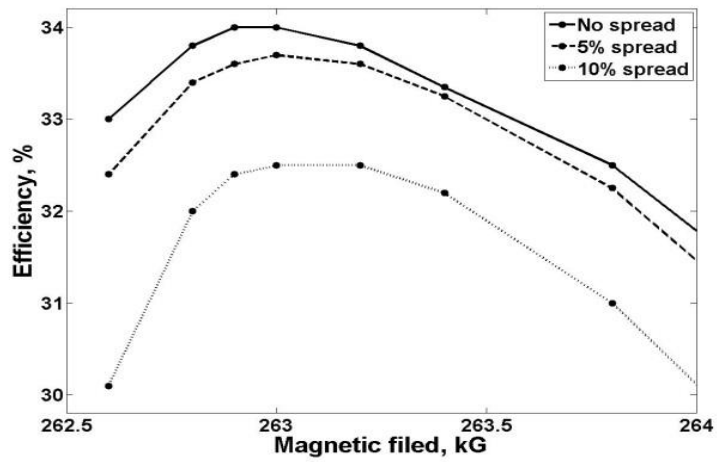

Figure 9 (b) Efficiency for Profile 2

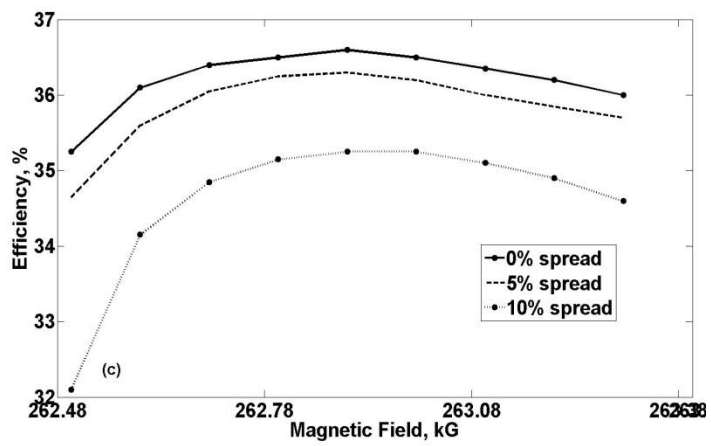

Figure 9 (c) Efficiency for Profile 3

Aside from the single mode calculation, we also performed MAGY calculation for multimode interaction. Cold cavity simulations have shown that there is weak mode conversion of about 1% of the power of the cavity mode that occurs at the tapering near the input and the output of the interaction circuits. These simulations showed that there are no serious mode competitions inside the cavity between the neighboring radial modes. Simulations also showed that potential depression due to DC space charge field has negligible effect on the overall efficiency. In fact, change in the beam potential due to space charge is less than 1 V for our current and voltage.

Plasma Break Down

Once the THz beam creates air breakdown, plasma will be formed in the breakdown region. When the electron density is high enough, a significant part of the wave beam should be reflected from dense plasma, and therefore can be registered by an observer located close to the source of THz radiation.

I plan to address the issue of THz reflection from breakdown volume for reflection source that is on the order of wave length. The results of this study may help to shed light on the possibility of using modern detectors that can resolve signals at this wavelength at microwatt level. Some experiments similar to our case were carried out at MIT with a 110 GHz gyrotron, where the plasma filamentation in a gyrotron focused wave beam was observed [16] [17]. Also a recent Russian experiment with a THz gyrotron created plasma using focused THz wave beam [18].

The study is planned to be carried out by developing analytical equations based on scattering off a plasma object shaped as shown in figure 10, where the plasma frequency calculated from excess power density over threshold hold in the course of ionization. The plasma density inside the volume is approximate by $n = n_0 \exp\left(\nu_{i,eff} t\right)$, where $\nu_{i,eff}$ is the effective ionization frequency, obtained using a Fokker-Plank kinetic code in [5], and is dependent on the power density over power threshold density.

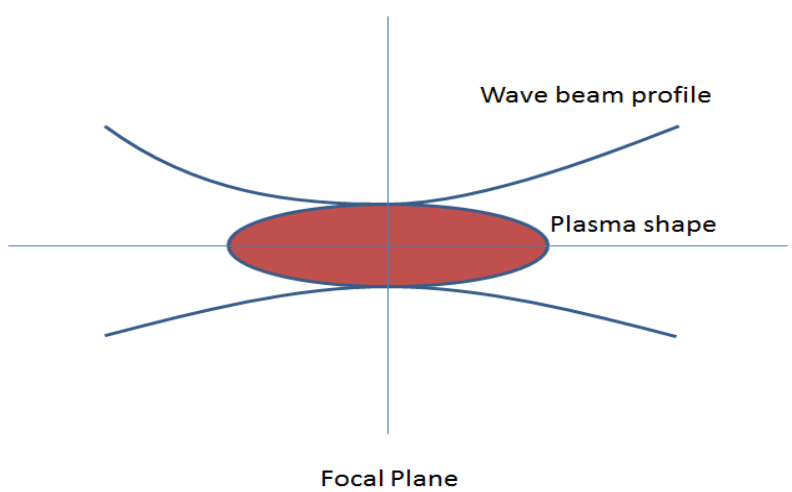

Figure 10 shape of the plasma density region

From these to starting points, the future plan is to investigate the temporal behaviors of the plasma volume using equations, and find out the viability of using the reflected signal from the gyrotron to determine characteristic of the breakdown events.

Gyrotron Theories

Guiding Center Spread

Conventional gyrotrons have axially symmetric interaction spaces. Gyrotron electron beams can be thought of as thin annular beams that are distributed about the center axis, while electrons themselves gyrate with Larmor radius, see figure 11. The effect of the beam displacement on the gyrotron operation was studied in [19] [20]. The effects of the beam thickness, which is defined as the spread of guiding center for small orbit gyrotron, were only studied in mode interaction [21]. The effects of this spread were typically neglected in gyrotron development, mostly due to the fact that development has been focused on frequencies less than 200 GHz [22] [23]. At those wavelengths, it is straightforward to design a magnetron injection gun with a thin emitter and electro-optic system that limit the guiding center spread to typically less than 1/6 of the wave length [24] [25]. For a 670 GHz gyrotron however, the magnetic field compression ratio would be much higher. Having a thin emitter width presents design difficulties, where the area of the emitter is proportional to $f^{-4/3}$, f is frequency. We believed it was important to see how much spread can exist without compromising efficiency.

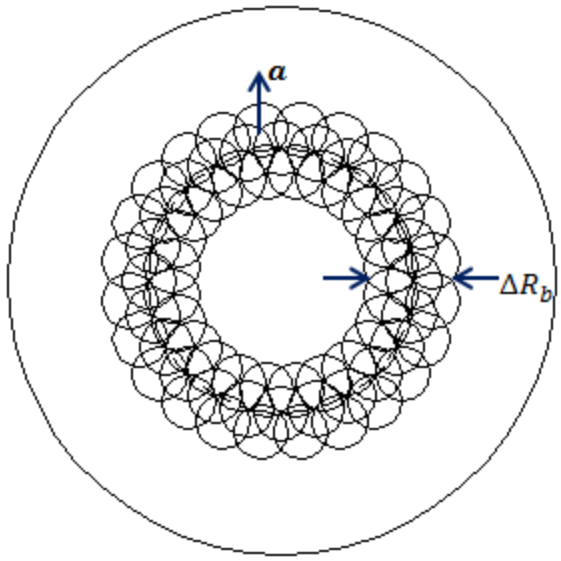

Figure 11 a is the Larmor radius, Δ R is the guiding center spread.

The radius of electron guiding centers in the resonator (beam radius R_b) should provide maximum electron coupling to the desired mode. This coupling is determined by the function

$$G_{m,p} = \frac{J^2_{m\mp s}\left(\nu_{m,p} R_b / R_w\right)}{\left(\nu^2_{m,p} - m^2\right) J^2_m\left(\nu_{m,p}\right)}$$

It depends on the beam-to–wall radius ratio as shown in figure 12 for the $TE_{31,8}$-mode co-rotating with the direction of electron gyration (In the case of a co-rotating mode the index of the Bessel function in the numerator should be taken with the sign 'minus' ($m - s$). As follows from figure 12, the optimal beam radius is equal to 0.51 of the wall radius, i.e. it is equal to 2.3 mm, and the maximum coupling coefficient defined by above equation for this mode is approximately equal to $1.3 \cdot 10^{-3}$.

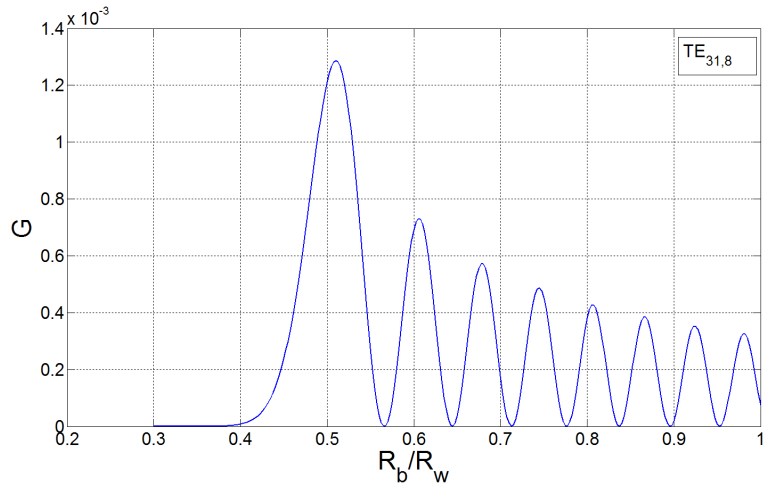

Figure 12 Coupling factor of the TE31,8-mode

In the paper we published on this matter [26], the analytical theory is developed that allows one to estimate the effect of electron spread in guiding center radii on the gyrotron efficiency. The analytical theory is built on polynomial approximations of dependence of gyrotron efficiency on wave amplitude in the resonator cavity, with different expressions for cases where the gyrotron operates in soft and hard self-excitation regime.

In general, the results of this theory agree reasonably well with numerical results we obtained with the use of the self-consistent code [15], as shown in figure 13. The two curves are predictions from the analytical expressions, and the data points are numerical results. It shows that the gyrotron operation is less sensitive to the spread when the device is in the region of soft self-excitation than in the region of hard excitation. Soft self-excitation refers to regime where the beam current is above the start oscillation current, and the RF amplitude grows from noise level. Hard self-excitation is the regime where the beam current far exceeds the start oscillation current, and it only takes place if the initial amplitude is above a certain threshold. The figure also shows that the gyrotron operation is less sensitive to this spread when the beam is injected in the inner peak of the function describing the beam coupling to the wave. In this case, even the spread of about one third of the wavelength reduces the gyrotron efficiency by about 10% or less of its nominal value (i.e. such a gyrotron with a relatively “thick” beam can operate with the interaction efficiency of 27% versus 30% achievable in a gyrotron with ideally thin beam). For THz-range gyrotron, it is possible to double the emitter width while keeping the efficiency high, this lessens the restriction on gun design.

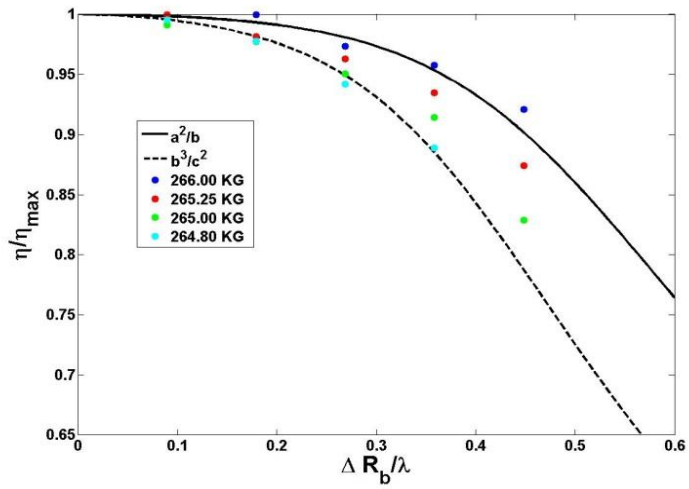

Figure 13 Efficiency with respect to ideal beam (zero spread). The lines represent our theories. Solid line corresponds to expression describing soft self-excitation, dashed line corresponds to hard self-excitation. The dots are results of MAGY simulation

Frequency Tunability

One possible feature of interest in other possible applications for the proposed terahertz gyrotron that was explored is frequency tunability [27]. We approach this problem by studying interaction circuits with tapered wave guide, as similar idea had been proposed before in [28]. A more developed theory of a gyrotron backward-wave oscillator with tapered parameters was conceived in [29], but it is limited to excitation condition far from cut-off. Our study tries to expand the theory in [29] to a wider range of cut-off conditions.

Self-consistent equation sets for gyro devices consist of equations for the electron beam and equation for the EM fields. Under the small signal theory, EM field amplitude can be treated as a small parameter, and equations of electron motion in external magnetic field and small EM amplitude can be linearized with respect to EM perturbations. This reduces the equation set into linear equations that define the start oscillation current for a gyrotron [12].

The axial field profile term in that equation can be approximated by the use of Airy Functions in a tapered wave guide, as shown in figure 14 below, where α_t is the tapering angle. By adjusting the cyclotron detuning and exciting waves with large number of axial variations, one can introduce different resonance curves inside the tapered wave guide. The overlaps of these resonance modes, described in [30], will create large frequency tunability, which have already been seen in experiments [9] [31].

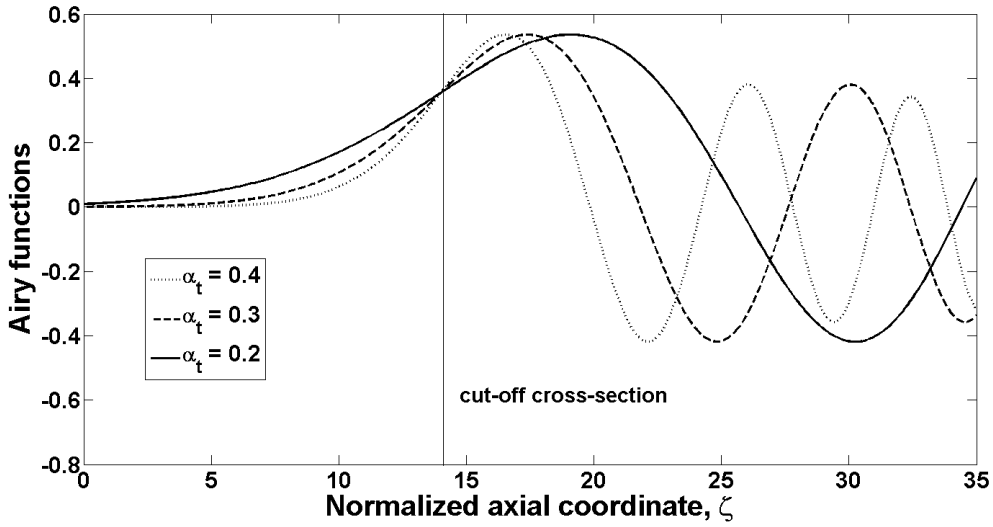

Figure 14 Airy function approximation of axial field profile

Furthermore, in this study we used the linear equations to estimate various normalized start oscillation current for different tapering angles. The results are shown in figure 15,

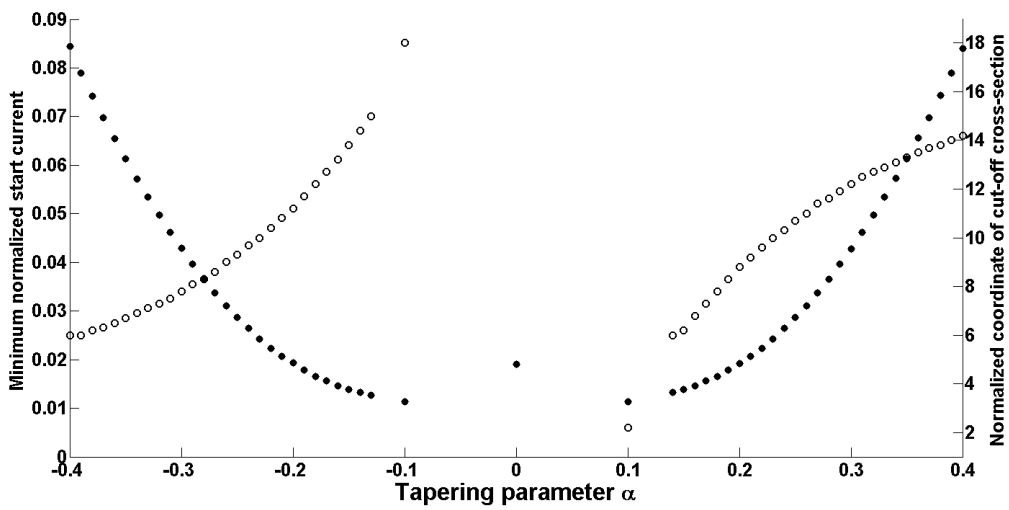

Figure 15 Minimum normalized start current (solid circles) and corresponding coordinates of the cutoff cross-section (empty circles) as functions of the tapering parameter.

The minimum normalized start current was calculated assuming the optimal cyclotron detuning and a normalized length of 20. The position of cut-off cross section relates to the tapering angle, and from that the cut-off radius can be determined and cut-off frequency can be estimated using the Airy

function approximation of field profile. At zero angle, the field was approximated by sine waves with four and five axial peaks.

Second Harmonic Interaction

As mentioned before, the frequency of gyrotron oscillators are directly proportional to the strength of magnetic field. Figure 2 shows that in order to reach 1THz at the fundamental cyclotron harmonic, the field required is close to 40 Tesla.

One approach to increase gyrotron frequency without the limitation of the magnetic field supply is to operate the gyrotron in higher cyclotron harmonic. Nonlinear effects in the mode interaction puts the higher harmonic gyrotrons at a disadvantage, where the fundamental modes can become the dominate mode and suppress the desired second harmonic mode.

Previous studies [32] [33]have tackled this problem. It has been mentioned that the second harmonic mode, once excited can stay the dominate mode. To expand further on that work, we plan to use simple gyrotron equation to find the parameter range in which the second harmonic can stay the dominant mode in steady state operation. By solving the gyrotron equations for different sets of cyclotron detuning for each mode, one can find a region of magnetic field where the nonlinear mode interactions would favor the second harmonic operation. Once the detuning information is gathered from the simple equations, MAGY simulations will be used to confirm the results.

Summary

As of now, I have completed the study on frequency tunability, effect of guiding center spread and the cavity design. On the second harmonic mode interaction and THz wave beam reflection I have made partial progress and I am on track to complete both works in time for my graduation. My works at the University of Maryland will hopefully add to the overall knowledge of the international gyrotron research.

Work Cited

[1] V. L. Granatstein and G. S. Nusinovich, *J. Appl. Phys,* vol. 108, no. 6, pp. 1-5, 2010.

[2] G. S. Nusinovich, R. Pu, T. M. Antonsen Jr., O. V. Sinitsyn, J. Rodgers, A. Mohamed, J. Silverman, M. Al-Sheikhly, Y. S. Dimant, G. M. Milikh, M. Y. Glyavin, A. G. Luchinin, E. A. Kopelovich and V. L. Granatstein, *J Infared Milli Terahz Waves,* vol. 32, no. 3, pp. 380-402, 2010.

[3] Technical report, "Nanosecond pulse breakdown initiation and growth," RADC-TDR-63-525, 1964.

[4] A. G. Litvak, "Freely Localized Gas Discharge in Microwave Beams," in *Application of High Power Microwaves*, A. V. Gaponov-Grekhov and V. L. Granatstein, Eds., Norwood, MA: Artech House, 1994.

[5] G. S. Nusinovich, G. M. Milikh and B. Levush, *J. Appl. Phys,* vol. 80, p. 4189, 1996.

[6] A. A. Negirev and A. S. Fedorov, *Radiotekhnika,* no. 4, p. 41, 1999.

[7] V. A. Flyagin, A. G. Luchinin and G. S. Nusinovich, *Int. J. Infared Millim. waves,* vol. 4, no. 4, pp. 629-637, 1983.

[8] M. Y. Glyavin and A. G. Luchinin, *Terahertz Science and Technology,* vol. 2, no. 4, pp. 150-155, 2009.

[9] M. K. Hornstein, V. S. Bajaj, R. G. Griffin, K. E. Kreischer, I. Mastovksy, M. A. Shapiro, J. R. Sirigiri and R. J. Temkin, *IEEE Trans. Electron Devices,* vol. 52, pp. 798-807, 2005.

[10] M. Y. Glyavin, A. G. Luchinin, V. N. Manuilov and G. S. Nusinovich, *IEEE Trans. Plasma Sci.,* vol. 36, pp. 591-596, 2008.

[11] G. L. Carr, M. C. Martin, W. R. McKinney, K. Jordan, G. R. Niel and G. P. Williams, *Nature,* vol. 420, p. 153, 2002.

[12] G. S. Nusinovich, Introduction to the Physics of Gyrotrons, Baltimore: Johns Hopkins University Press, 2004.

[13] G. S. Nusinovich, P. Sprangle, C. A. Romero-Talamas and V. L. Granatstein, *J. Appl. Phys.,* vol. 8, no. 109, p. 3303, 2011.

[14] K. Sakamoto, A. Kasugai, R. Minami, N. Kobayashi and K. Kajiwara, *Nat. Phys. ,* vol. 3, p. 411, 2007.

[15] M. Botton, T. M. Antonsen Jr., B. Levush, K. T. Nguyen and A. N. Vlasov, *IEEE Trans. Plasma Sci.,* vol. 26, pp. 882-892, 1998.

[16] Y. Hidaka, E. M. Choi, I. Mastovsky, M. A. Shapiro, J. R. Sirigiri and R. J. Temkin, *Phys. Rev. Lett,* vol.

3, no. 100, p. 5003, 2008.

[17] A. Cook, M. A. Shapiro and R. J. Temkin, *Appl. Phys. Lett,* vol. 97, no. 1, p. 1504, 2010.

[18] V. L. Bratman and et al, *Phys. Plasmas,* vol. 18, no. 8, p. 3507, 2011.

[19] O. Dumbrajs and L. Shenggang, *IEEE Trans. Plasma Sci.,* vol. 20, p. 126, 1992.

[20] G. S. Nusinovich, O. Dumbrajs and B. Levush, *Phys. Plasma,* no. 2, p. 4621, 1995.

[21] G. S. Nusinovich, O. V. Sinitsyn, M. Yeddulla, L. Velikovich, T. M. Antonsen Jr., A. N. Vlasov, S. Cauffman and K. Felch, *Physics. Plasmas ,* no. 10, p. 3335, 2003.

[22] K. L. Felch, B. G. Danly, H. R. Jory, K. E. Kreischer, W. Lawson, B. Levush and R. J. Temkin, *Proc. IEEE,* vol. 87, p. 752, 1999.

[23] K. Sakamoto, *Fusion Sci. Technol.,* vol. 52, p. 145, 2007.

[24] J. M. Baird and W. Lawson, *Int. J. Electron,* vol. 61, p. 953, 1986.

[25] K. Felch, D. Stone, H. Jory, R. Gracia, G. Wendell, R. J. Temkin and K. E. Kreischer, in *Int. Electron Devices Meet*, San Fransisco, 1982.

[26] R. Pu, G. S. Nusinovich, O. V. Sinitsyn and T. M. Antonsen Jr., *Physics. Plasmas,* vol. 17, p. 3105, 2010.

[27] G. S. Nusinovich, R. Pu, O. V. Sinitsyn, J. Yu, T. M. Antonsen Jr. and V. L. Granatstein, *IEEE Trans. Plasma Sci.,* vol. 38, no. 6, p. 1200, 2010.

[28] V. L. Bratman, S. L. Novozhilov and M. I. Petelin, *Elektronnaya Tekhnika,* no. 11, pp. 46-49, 1976.

[29] G. S. Nusinovich and O. Dumbrajs, *IEEE Trans. Plasma Sci.,* vol. 24, no. 3, pp. 620-629, 1996.

[30] J. Zhao, G. S. Nusinovich, H. Guo, J. Rodgers and V. L. Granatstein, *IEEE Trans. Plasma Sci.,* vol. 28, no. 3, pp. 597-605, 2000.

[31] H. Guo, S. H. Chen, V. L. Granatstein, J. Rodgers, G. S. Nusinovich, M. Walters, B. Levush and W. J. Chen, *Phys. Rev. Lett.,* vol. 79, no. 3, pp. 515-518, 1997.

[32] S. H. Kao, C. C. Chiu, K. F. Pao and K. R. Chu, *Phys. Rev. Lett,* no. 13, p. 5101, 2011.

[33] I. G. Zarnitsyna and G. S. Nusinovich, *Radiophysics & Quantum Electronics,* no. 20, pp. 313-317, 1977.